RILEM Technical Letters (2017) 2: 67-73
DOI: http://dx.doi.org/10.21809/rilemtechlett.2017.35

# Rate controls on silicate dissolution in cementitious environments

Tandre Oey[a,b], Yi-Hsuan Hsiao[a,b], Erika Callagon La Plante[a,b], Bu Wang[a,b], Isabella Pignatelli[a,c], Mathieu Bauchy[d], Gaurav Sant[a,b,e*]

[a] Laboratory for the Chemistry of Construction Materials (LC$^2$), Department of Civil and Environmental Engineering, University of California, Los Angeles, CA 90095, USA
[b] California Nanosystems Institute, University of California, Los Angeles, CA 90095, USA
[c] Laboratory for Georesources, Faculté des Sciences et Technologies, Campus des Aiguillettes, Vandoeuvre-lès-Nancy CEDEX, France
[d] Laboratory for the Physics of Amorphous and Inorganic Solids (PARISlab), Department of Civil and Environmental Engineering, University of California, Los Angeles, CA 90095, USA
[e] Department of Materials Science and Engineering, University of California, Los Angeles, CA 90095, USA

Received: 03 July 2017 / Accepted: 25 December 2017 / Published online: 30 December 2017


## Abstract

The dissolution rate of silicate minerals and glasses in alkaline environments is of importance in cementitious systems due to its influences on: (a) early-age reactivity that affects the rate of strength gain and microstructure formation, and/or, (b) chemical durability of aggregates; compromises in which can result deleterious processes such as alkali-silica reaction (ASR). In spite of decades of study, quantitative linkages between the atomic structure of silicates and their dissolution rate in aqueous media (i.e., chemical reactivity) has remained elusive. Recently, via pioneering applications of molecular dynamics simulations and nanoscale-resolved measurements of dissolution rates using vertical scanning interferometry, a quantitative basis has been established to link silicate dissolution rates to the topology (rigidity) of their atomic networks. Specifically, an Arrhenius-like expression is noted to capture the dependence between silicate dissolution rates and the average number of constraints placed on a central atom in a network ($n_c$, i.e., an indicator of the network's rigidity). This finding is demonstrated by: (i) ordering fly ashes spanning Ca-rich/poor variants in terms of their reactivity, and, (ii) assessing alterations in the reactivity of albite, and quartz following irradiation due to their potential to induce ASR in concrete exposed to radiation, e.g., in nuclear power plants.

**Keywords:** Silicates; Cement; Concrete; Reactivity; Durability

## 1 Introduction and background

The dissolution rates of silicate solids including minerals and glasses, in alkaline environments, is of great relevance in cementitious systems. For example, the dissolution behavior of $Ca_3SiO_5$ ($C_3S$), the primary component in ordinary portland cement (OPC) is well-known to influence aspects ranging from early-age heat release, to microstructure formation and strength development [1-9]. On the other hand, due to the significant $CO_2$ emissions intensity of OPC there is substantial emphasis on replacing OPC by other supplementary cementitious materials (SCMs, e.g., slags, fly ash and calcined clays) in the binder fraction in concrete [10-15]. While it is desirable to select an OPC replacement agent with similar hydraulic reactivity (i.e., dissolution rate in water) as OPC, this is most often infeasible. However, simply, it could be suggested that an optimal OPC replacement agent is one that offers the smallest decrement in hydraulic reactivity vis-à-vis OPC. This may suggest that optimal OPC replacement agent(s) can be identified by ranking/ordering potential SCMs such as fly ash in terms of their dissolution rates [16,17]; an effort which is not implemented currently. This is because our ability to forecast binder performance based on knowledge of its composition and the (atomic) structure of its constituents is lacking. In an alternate scenario, deleterious reactions such as alkali-silica reaction (ASR) which degrade concrete's durability are known to manifest due to the presence of reactive siliceous aggregates, i.e., which will dissolve in high pH environments [18-21]. However, even now, we lack a robust ability to utilize aggregate dissolution rates (or surrogate descriptors) to classify ASR risks along a spectrum ranging from high (reactive aggregate)-to-low (inert aggregate). As such, in spite of silicate dissolution being a topic of central importance to not only "cement science" but also the broader concrete construction industry, our understanding of silicate dissolution is yet far from mature. Therefore, this letter builds on our understanding of silicate dissolution (kinetics) in alkaline environments with special focus on establishing linkages between atomic structure and the

* Corresponding author: Gaurav Sant, Tel. (310) 206-3084, E-mail: gsant@ucla.edu

chemical reactivity of silicates (i.e., as described by their aqueous dissolution rate). This new understanding offers quantitative ability to estimate, and predict silicate reactivity, and describe such behavior within a consistent thermodynamic framework that captures the atomic architecture of cementitious, and related materials.

## 2 Materials

Seven commercially available fly ashes were sourced to encompass a range of compositions of abundant U.S. fly ashes (and coal streams). This includes three Class C ("Ca-rich") fly ashes, and four Class F ("Ca-poor") fly ashes as per ASTM C618 [22]. The detailed compositions of the fly ashes, in terms of their mineralogy and bulk oxide compositions are noted elsewhere [16]. While X-ray fluorescence (XRF) was used to establish bulk oxide compositions, quantitative X-ray diffraction (QXRD) using ZnO as an internal standard and Rietveld refinement analyses was used to establish the crystalline compounds present. X-ray structure information for relevant anhydrous and hydrated crystalline phases was taken from the literature or standard databases. The average composition of the glassy components in each fly ash was established by subtracting the QXRD-based compositions of the crystalline compounds from the XRF-based total (simple) oxide compositions [16].

Synthetic single crystals of α-quartz were sourced from MTI Corporation [23,24]. The quartz crystals are (001)-oriented. In addition to these single crystals, an untreated fumed silica (CAB-O-SIL HS-5), a size graded, pulverized α-quartz (MIN-U-SIL 10), albite sections which were sourced from Ward's Natural Science Company [25,26], and synthetic borosilicate [27] and aluminosilicate glasses [28] (i.e., the latter with compositions equivalent to the *average glass* present in the commercial fly ashes) were also examined. The (001) quartz and albite samples were ion-beam irradiated at room temperature at the Michigan Ion Beam Laboratory (MIBL [29]) using an implantation energy of 400 keV with $Ar^+$-ions to a total fluence of $1.0 \times 10^{14}$ ions/cm$^2$. No signs of any blistering or of any sputtering were observed post-irradiation. Based on these implantation characteristics, the disordered mineral zone is estimated to be on the order of 600 nm deep, based on knowledge of the mineral density, and calculations carried out using the package: The Stopping and Range of Ions in Matter (SRIM) [30].

## 3 Methods

***Vertical scanning interferometry (VSI) for measuring aqueous dissolution rates:*** The *average* dissolution rates of the fly ash, mineral, and glass samples were measured at room temperature (298 K) using vertical scanning interferometry (VSI) [31,32]. VSI offers the ability to acquire three dimensional-visualizations of reacting surface topographies with nanoscale vertical resolution (≈1-2 nm) over sample areas on the order of 10s of mm$^2$. Importantly, by directly tracking the surface retreat (i.e., change in height vis-à-vis an unchanging reference) following solution contact as a function of time, VSI reveals nanoscale resolved dissolution rates [33,34]. This method has significant advantages over other methods that are based on the analysis of solution compositions. For example, dissolution rates obtained from VSI do not require normalization to the surface area of the reacting solid. Furthermore, VSI measures the surface retreat rates, which can be directly related to molar dissolution through the molar volume, while being indifferent to the fate of dissolved species, and the stoichiometry therein (e.g., due to potential incongruencies in dissolution).

In general, dissolution rates were quantified whereby: (i) a collection of (fly ash) particles were embedded in an inert substrate, or (ii) a planar mineral/synthetic glass surface that is partially covered with an inert silicone film (i.e., "masked", see Fig.1(a) are submerged in a static drop or fixed volume of solution for a prescribed time interval [16,32,35-38]. In all cases, a high liquid-to-solid mass ratio (l/s, ≥ 500) is used with contact times ranging on the order of minutes (glasses) to hours (albite) depending on the solid's aqueous dissolution rate. The solvent is evacuated using a compressed $N_2$ gas stream between "raindrop" or immersion cycles. Solution pH's ranging between 10-to-14.6 were achieved by dissolving reagent grade sodium hydroxide (NaOH, to simulate the presence of alkalis in cement and/or fly ash) in deionized (DI) water (18 MΩ·cm).

Since fly ashes consist of both glassy and crystalline compounds, data collection was initiated after the first 15 minutes of contact with the solution. The delay in data collection was necessary to ascertain the dissolution rate of only the glassy compounds present in the fly ash, while minimizing interference from the fast dissolving crystalline compounds such as $Ca_3Al_2O_6$ ($C_3A$) that may be present [39,40]. It should be noted that the interactions of compounds such as quartz that are often present in fly ash with the solution are irrelevant because their dissolution rates are far lower (i.e., by several orders of magnitude) than those of the glassy components in fly ash [41,42]. The dissolution rates of the fly ashes are taken from the average of 50-120 different subsets of particles as noted in detail elsewhere [17].

In all cases, the imaging was carried out such that a "reference area" was identified, i.e., either the inert polymer substrate in the case of fly ash particles, or the unreacted area previously covered by the silicone mask in the case of the planar sections. As a result, the "reference area" remains unaffected upon contact with the solution, while other areas dissolve thereby showing a reduction (retreat) in height. The VSI images thus acquired after nulling the surfaces (i.e., to compensate for sample tilt, if any) were analyzed to assess the change in height of the dissolving surface, with respect to the unchanging reference as a function of the time. The change in height, h, as a function of time, t, ($\Delta h/\Delta t$) when normalized by the molar volume of the solid yields its molar dissolution rate.

***Molecular dynamics (MD) simulations for assessing the network rigidity:*** The structure of the glassy components present in the fly ashes, or of the synthetic boro-/alumino-silicate glasses was assessed via molecular dynamics (MD) simulations in LAMMPS [46]. The composition of the

simulated systems was restricted to the following oxides: $SiO_2$ and $Al_2O_3$ (network forming species), and CaO, MgO, $Na_2O$, and $K_2O$ (network modifying species). MD simulations of the glasses were then performed utilizing the conventional melt-quenching method at zero pressure in the *NPT* ensemble as follows: (1) heating the system to 4000 K to remove any memory of its initial atomic configuration, (2) cooling to 300 K at a rate of 1 K/ps, (3) relaxing the structure at 300 K for an additional 100 ps, and (4) equilibrating the structure for an additional 100 ps in the *NVT* ensemble for statistical averaging [47]. The simulations were performed with a time step of 1 fs using the interatomic potential parametrized by Teter [48].

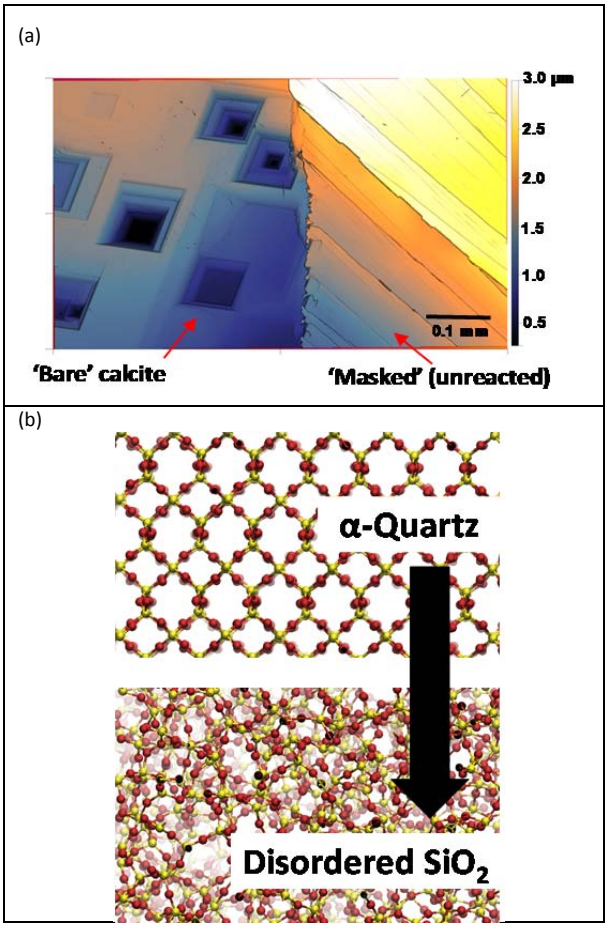


**Figure 1.** (a) A representative VSI-resolved image of a dissolving calcite (104) surface cleaved from a single crystal that shows the presence of etch pits that propagate deeper into the solid in stepwaves (e.g., see [43]) with increasing dissolution. The dissolution measurements were carried out at pH 5.6 (in DI-water, 18 MΩ·cm in equilibrium with air) at 298 K for 15 h wherein a portion of the calcite surface was masked by an inert silicone film and an adjacent area was permitted to dissolve (react). The change in height of the unmasked area vis-à-vis the unmasked reference reveals the dissolution rate ($K = \Delta h/\Delta t$, where K is the dissolution rate, and h and t denote height and time, respectively). This image was rendered using Gwyddion [44]. (b) The evolution of α-quartz's periodic (crystalline) structure into disordered silica under energetic particle exposure (red: oxygen atoms, yellow: silicon atoms). The input α-quartz structure was sourced from Levien et al. [45] and the disordered structure that results following energetic particle exposure was established via MD simulations [32]. The MD simulations considered an incident particle energy of 600 eV for a computational volume consisting of 8100 atoms.

MD simulations of irradiation-induced structural alterations in albite and α-quartz were carried out following the methodology of Wang et al. [24,49]; e.g., see Fig. 1(b) for irradiation induced disordering of α-quartz. The crystal structures of pristine albite and α-quartz sourced from Armbruster et al. or Levien et al. respectively, offered the initial atomic configurations [45,50]. To simulate the effects of irradiation, an atom, randomly chosen from the mineral's structure was accelerated with a kinetic energy equivalent to that of an incident neutron – selected to be 600 eV herein. The accelerated atom then collides with other atoms, thereby resulting in a ballistic cascade. A spherical region with a radius of 10 Å is subsequently created around the primary knock-on atom (PKA), outside which all atoms are kept at a constant temperature of 300 K by a Berendsen thermostat [51]. In contrast, the dynamics of the atoms inside the sphere are treated within the *NVE* ensemble to avoid any spurious effects of thermostat. The dynamics of the cascade is simulated for 15 ps, which was found to be long enough to ensure the convergence of both temperature and energy of the system. After each collision, the system is relaxed within the *NPT* ensemble at 300 K and zero pressure for another 5 ps. This enables the system to equilibrate its density following irradiation. This process is repeated iteratively with different knock-on atoms, until the system exhibits saturation in terms of its enthalpy and density [49]. A Buckingham potential parameterized by Teter and splined with the Ziegler-Biersack-Littmark (ZBL) potential was used to ensure realistic short-range repulsive interactions during the ballistic cascades [52].

The structures of the glasses, and the pristine and irradiated minerals were analyzed within the framework of topological constraint theory (TCT); also known as rigidity theory [53-55]. TCT captures the relevant features of the atomic topology which influence the kinetics of solid dissolution [35], while filtering out less relevant structural details. This is achieved by simplifying complex atomic networks into simple mechanical trusses, wherein the nodes (i.e., the atoms) are connected to each other through constraints (i.e., chemical bonds): the radial bond-stretching (BS) and angular bond-bending (BB) constraints. The average number of constraints per atom ($n_c$) was determined via MD simulations [56,57], wherein the radial and angular excursions of the neighbors of each atom are computed to enumerate the BS and BB constraints, respectively.

## 4 Results and discussion

Figure 2(a) shows the dissolution rates of a range of Ca-rich and Ca-poor fly ashes across a range of pH levels. In general, it is noted that the dissolution rates of the different fly ashes: i) increase with solution pH, i.e., with an increase in $OH^-$ activity, and, ii) decrease with an increase in the solid's number of constraints. This latter scaling follows that of glass hardness, wherein solids which are overconstrained ($n_c > 3$) show a higher hardness than their isostatic ($n_c = 3$) or their underconstrained ($n_c < 3$) counterparts [58,59]. Expectedly in the high pH ranges considered herein, the dominant driving force for fly ash (and more generally, silicate solid)

dissolution arises from nucleophilic attack of tetrahedral $[SiO_4]^{4-}$ or $[AlO_4]^{5-}$ units present in the solid by $[OH^-]$ species sourced from an alkaline solvent. It should also be noted that the Ca-poor fly ashes show dissolution rates which are lower than their Ca-rich counterparts; although the correlation between the Ca-content in the fly ash and dissolution rates is not very strong. It should be noted that the $n_c$ parameter featured in Figure 2(a) is relevant to the entire fly ash glass, including both the network formers and modifiers; as also considered by the "network ratio" parameter proposed by Oey et al. [16].

The exponential dependence between dissolution rates and the number of constraints is also preserved when the range of solid compositions is expanded beyond fly ash to encompass synthetic borosilicate and aluminosilicate glasses (i.e., including partially and fully compensated variants), and pristine α-quartz. Indeed, fitting of the dissolution rate-$n_c$ data in Fig. 2(a-b) to an exponential expression of the form $K = K_0\exp(-n_cE_0/RT)$, where, K is the dissolution rate (mmol/$m^2$/s), $K_0$ is a dissolution rate constant that depends only on the solvent composition (i.e., dominantly the pH; mmol/$m^2$/s), $n_c$ is the number of atomic constraints per atom (unitless), $E_0$ is the amount of energy needed to rupture a unit atomic constraint (kJ/mole), R is the gas constant and T is the thermodynamic temperature (K) reveals that, at 298 K, $E_0 = 23 \pm 5$ kJ/mole. This estimate of $E_0$ which is derived from consideration of not only heterogeneous (fly ash) glasses that are produced during an uncontrolled, quenching process, but also of homogenous silicate solids across a wide compositional spectrum is similar to the value of 25.5 kJ/mole previously estimated for stoichiometric and fully-compensated aluminosilicate glasses and pure silicate solids by Pignatelli et al. [35].

The similarity in the values of $E_0$ across compositionally homogenous and heterogeneous solids, including those containing network modifiers suggests that the constraint rupture energy is dominated by the network formers (e.g., $[SiO_4]^{4-}$ and/or $[AlO_4]^{5-}$); albeit with smaller but relevant contributions that arise from the presence and distributions of modifier atoms. This indicates that (alumino)silicate dissolution rates are primarily dictated by the energy of bond rupture among $[SiO_4]^{4-}$ or $[AlO_4]^{5-}$ units – that is, the network forming species – wherein the average energy to liberate a network forming unit from the network is given by $E_a = n_cE_0$ [35]; where $E_a$ is the activation energy (kJ/mole). The estimation of the activation energy of the rate controlling process in dissolution is suitably captured by the "topological prediction" as shown in Figure 2(c) which shows experimental determinations of the activation energy of silica and quartz dissolution as compared to the topological prediction, wherein $E_a = n_cE_0$ (N.B.: $n_c = 3.00$ and 3.67 for silica and quartz respectively, and $E_0 = 23 \pm 5$ kJ/mole). This established dependence of dissolution rates on the number of atomic constraints is shared by other dynamic processes including ion diffusion and conduction, and suggests that the three relevant mechanisms involved in dissolution, i.e., hydration, hydrolysis, and ion-exchange (e.g., see Fig. 2c [35]), can be formalized within a consistent thermodynamic framework which encompasses the material's architecture, i.e., arrangement of atoms as described by the network's topology.

In a different albeit related context, at a constant composition, external stimuli ("shock") in the form of temperature and pressure impositions, and irradiation can alter the network topology of a solid, e.g., from the crystalline to increasingly disordered states [26,32,49]. This nature of alterations which may occur, e.g., when minerals

are exposed to radiation in the form of neutrons in nuclear power plants, can alter the chemical durability of the mineral(s), and in turn, the surrounding concrete due to the potential onset of ASR in even otherwise unreactive aggregates [32,66-70]. In support of this idea, Figures 3(a-b) show the effects of alterations in network rigidity effected by ion-irradiation on the dissolution rates of albite and quartz in alkaline environments. It is noted that, consistently, heavy ion implantation using $Ar^+$ ions (i.e., equivalent to neutron irradiation when effected to the terminal disordered state [71,72]) results in an elevation in mineral dissolution rates. Indeed, while the dissolution rate of albite (Fig. 3a) elevates by up to 20x following irradiation, the dissolution rate of quartz elevates by up to 500x following irradiation, broadly for pH levels greater than 10 (pH units). Herein, it should be noted that although the atomic structure of terminally irradiated minerals differs from that of its compositionally equivalent glass (e.g., see [49]), radiation exposure does indeed result in the irradiated mineral and its equivalent glass featuring similar dissolution rates (e.g., see Fig. 3b for dissolution rates of glassy silica and irradiated quartz). Nevertheless, topological estimates which consider the change in the network rigidity ($\Delta n_c$, unitless) for albite and quartz, following irradiation taken as 0.307 and 0.77 respectively [32,38] (e.g., see Fig. 3c), indicate that the dissolution rates of these minerals would elevate on the order of 17x and 1000x respectively, when irradiation to the terminal disordered state is effected [32,38]. These estimates which yield a dissolution enhancement ratio (DER = $K_i/K_p = \exp[-\Delta n_cE_0/RT]$ where the subscripts 'i' and 'p' indicate the irradiated and pristine states respectively [38]), offer excellent agreement with experimental data when considering that $E_0 = 23 \pm 5$ kJ/mole across all scenarios considered. Taken together, these outcomes are significant not only because they provide a rational means to link irradiation- (or pressure- and temperature-) induced structural atomic alterations to changes in the chemical durability of minerals; but also because in the context of concrete construction as they provide a means to potentially rank, select, and screen different aggregate compositions (and supplementary cementitious materials; SCMs) in terms of their sensitivity, or lack thereof to deleterious processes such as alkali-silica reaction (ASR).

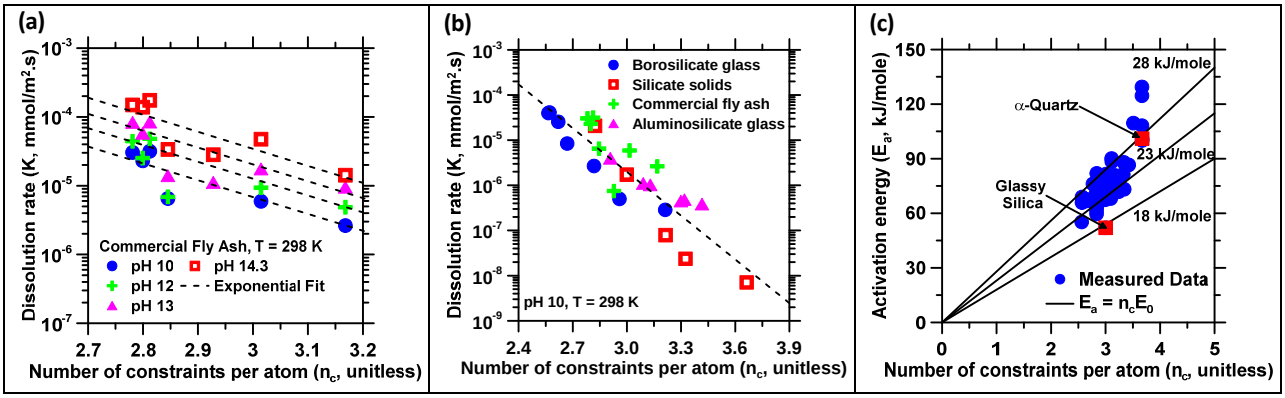


**Figure 2.** (a) The average dissolution rates of a range of Ca-rich and Ca-poor fly ashes as a function of the solution pH. The data is fitted by an exponential (*Arrhenius-like*) function of the form $K = K_0 \exp(-n_c E_0/RT)$ [16]. (b) The dissolution rates of synthetic borosilicate glass [27], silicate solids (i.e., including glassy variants of albite, jadeite and nepheline, pristine α-quartz, and soda-lime glass [60]), commercial fly ashes [17], and synthetic aluminosilicate glasses (i.e., with compositions similar to the average glass composition present in the commercial fly ashes) [28] as a function of the average number of atomic constraints ($n_c$) – for dissolution occurring at pH 10 at 298 K [28,30,43,61,62]. The slope of the linear regression in (a, b) reveals $E_0$, i.e., the energy required to break or rupture a unit atomic constraint, to be on the order of 23 ± 5 kJ/mole. **(c)** The measured activation energy of dissolution of glassy silica and α-quartz as a function of the number of constraints per atom [35]. The data are compared with measured activation energies of sodium silicate (i.e., for self-diffusion [60] and conduction [63] of Na), potassium silicate (i.e., for self-diffusion [63] and conduction [64] of K) fused silica (i.e., for the diffusion of water [64]), and quartz (i.e., for the diffusion of water [65]). The dashed line shows the predicted activation energy ($E_a$, kJ/mole) given by: $E_a = n_c E_0$ wherein $E_0$ takes values of: 18, 23, and 28 kJ/mole.

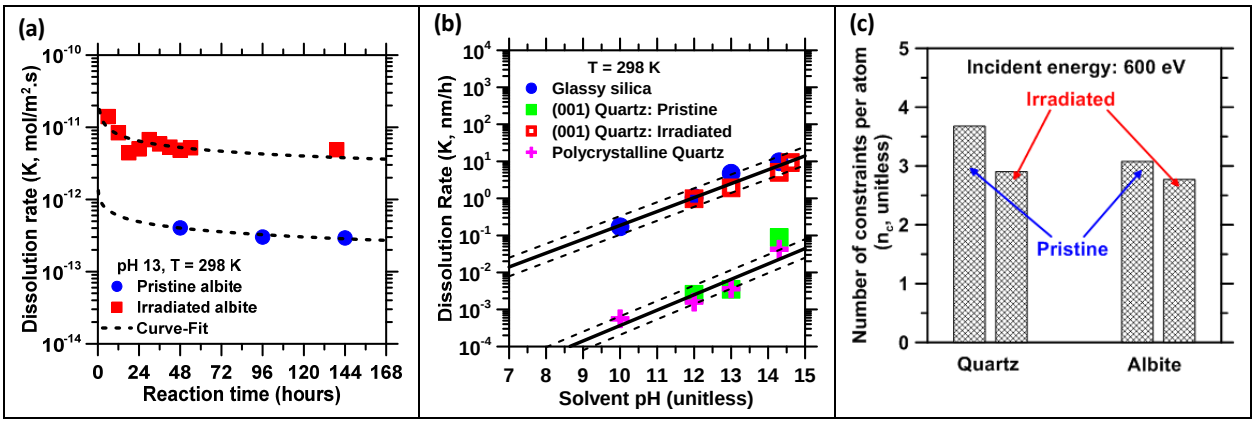


**Figure 3.** (a) A representative comparison of the dissolution rates of pristine and irradiated albite assessed using VSI as a function of time at pH 13 and 298 K. The dissolution rate of irradiated albite is nearly 20x higher than that of pristine albite as estimated from the change in the number of constraints of albite, following irradiation [38]. (b) The dissolution rate as a function of the solution pH for $SiO_2$-based solids including fumed silica, (001) surfaces of pristine and irradiated α-quartz, and polycrystalline α-quartz measured using VSI at 298 K [24]. The dissolution rate of α-quartz shows only slight sensitivity to surface orientation. The measured data are fitted by an equation of the form: $K = A \cdot \exp(\pm B \cdot pH)$, where A and B are numerical constants (the bold line shows fits, while the dashed lines show the uncertainty in the measurements). (c) The evolution of the average number of atomic constraints ($n_c$) in α-quartz and albite for an incident energy of 600 eV [24,26 ] as the minerals transition from their pristine (initial) to irradiated (final, disordered) states.

## 5 Summary and conclusions

The dissolution behavior of silicate solids is of great consequence to concrete performance; ranging from the fresh to the hardened states. However, our general understanding of the linkages between atomic composition and organization of solids, and their chemical reactivity has remained incomplete. In a series of comprehensive studies, researchers at UCLA have clarified that the dissolution behavior of silicate solids spanning disordered and crystalline domains can be resolved within a topological framework which considers the architecture ("rigidity") of atoms within a network. Indeed, careful quantifications of such network rigidity, accessed by MD simulations, when integrated with nanoscale-resolved measurements of silicate dissolution rates accessed using vertical scanning interferometry (VSI) highlight that silicate dissolution rates scale, in ascending order, with a decrease in network rigidity (i.e., described by the parameter $n_c$, which establishes the average number of constraints placed on a central atom within an atomic network). Such dissolution scalings which are captured by an exponential (*Arrhenius-like*) expression are demonstrated for solids including: commercially available fly ash, synthetic borosilicate and aluminosilicate glasses, crystalline silicates including quartz, and ion-implanted minerals including albite and quartz (i.e., wherein implantation is used as a means to

induce disorder at constant composition). Careful analysis of the scaling relation reveals the amount of energy that is needed to rupture a unit atomic constraint, $E_0$, i.e., noted to be on the order of 23 ± 5 kJ/mole across all solids considered. This is significant as it allows for the modeling and simulation of dissolution processes within a consistent thermodynamic framework that considers the amount of energy that is required to rupture the atomic network. In a more practical "concrete construction" context, the original dissolution scalings that are presented herein can not only help to rank and order fly ashes (and SCMs in general, e.g., slags and calcined slays) in terms of their chemical reactivity and hence suitability as cement replacement agents, but they also help establish the sensitivity of mineral aggregates to deleterious processes such as ASR. These outcomes offer a framework to reduce the construction industry's reliance on empirical knowledge for SCM and aggregate selection, and thereby have the potential to transition the industry's thinking to a robust, scientific basis for material selection, exploitation and durability estimation.

## Acknowledgements

The authors acknowledge financial support for this research provisioned by: the U.S. Department of Energy's Nuclear Energy University Program (DOE-NEUP: DE-NE0008398), the U.S. National Science Foundation (CAREER Award: 1253269), The Oak Ridge National Laboratory operated for the U.S. Department of Energy by UT-Battelle (LDRD Award Number: 4000132990), COMAX, a joint UCLA-NIST consortium that is supported by its industrial and government agency partners, and the U.S. Department of Transportation (U.S. DOT) through the Federal Highway Administration (DTFH61-13-H-00011). This research was conducted in the: Laboratory for the Chemistry of Construction Materials ($LC^2$), Laboratory for the Physics of AmoRphous and Inorganic Solids (PARISlab), and, Molecular Instrumentation Center (MIC) at UCLA. As such, the authors gratefully acknowledge the support that has made these laboratories and their operations possible. The contents of this paper reflect the views and opinions of the authors, who are responsible for the accuracy of the datasets presented herein, and do not reflect the views and/or policies of the funding agencies, nor do the contents constitute a specification, standard or regulation. GNS would also like to acknowledge Prof. Aditya Kumar (Missouri University of Science and Technology), Dr. Yingtian Yu (UCLA), Dr. Anoop Krishnan (IIT-Delhi), Dr. Yann Le Pape and Dr. Kevin Field (Oak Ridge National Laboratory), Dr. Jeffrey Bullard (National Institute of Standards and Technology) and Prof. Narayanan Neithalath (Arizona State University) for their collaboration and contributions to different aspects of this research.

## References

[1] J. W. Bullard, H. M. Jennings, R. A. Livingston, A. Nonat, G. W. Scherer, J. S. Schweitzer, K. L. Scrivener, J. J. Thomas, Mechanisms of cement hydration. Cem Concr Res (2011) 41: 1208–1223. https://doi.org/10.1016/j.cemconres.2010.09.011

[2] L. Nicoleau, M. A. Bertolim, Analytical model for the alite (C3S) dissolution topography. J Am Ceram Soc (2016) 99: 773–786. https://doi.org/10.1111/jace.13647

[3] J. W. Bullard, B. Lothenbach, P. E. Stutzman, K. A. Snyder, Coupling thermodynamics and digital image models to simulate hydration and microstructure development of Portland cement pastes. J Mater Res (2011) 26: 609–622. https://doi.org/10.1557/jmr.2010.41

[4] D. Damidot, A. Nonat, C3S hydration in diluted and stirred suspensions:(I) study of the two kinetic steps. Adv in Cem Res (1994) 6: 27-36. https://doi.org/10.1680/adcr.1994.6.21.27

[5] L. Nicoleau, A. Nonat, D. Perrey, The di- and tricalcium silicate dissolutions. Cem Concr Res (2013) 47: 14–30. https://doi.org/10.1016/j.cemconres.2013.01.017

[6] K. L. Scrivener, A. Nonat, Hydration of cementitious materials, present and future. Cem Concr Res (2011) 41: 651–665. https://doi.org/10.1016/j.cemconres.2011.03.026

[7] R. L. Berger, F. V. Lawrence, J. F. Young, Studies on the hydration of tricalcium silicate pastes II. strength development and fracture characteristics. Cem Concr Res (1973) 3: 497–508. https://doi.org/10.1016/0008-8846(73)90089-6

[8] F. V. Lawrence, J. F. Young, R. L. Berger, Hydration and properties of calcium silicate pastes. Cem Concr Res (1977) 7: 369–377. https://doi.org/10.1016/0008-8846(77)90064-3

[9] J. J. Chen, J. J. Thomas, H. F. W. Taylor, H. M. Jennings, Solubility and structure of calcium silicate hydrate. Cem Concr Res (2004) 34: 1499–1519. https://doi.org/10.1016/j.cemconres.2004.04.034

[10] V. G. Papadakis, S. Tsimas, Supplementary cementing materials in concrete. Cem Concr Res (2002) 32: 1525–1532. https://doi.org/10.1016/S0008-8846(02)00827-X

[11] M. Thomas, The effect of supplementary cementing materials on alkali-silica reaction: a review. Cem Concr Res (2011) 41: 1224–1231. https://doi.org/10.1016/j.cemconres.2010.11.003

[12] B. Lothenbach, K. Scrivener, R. D. Hooton, Supplementary cementitious materials. Cem Concr Res (2011) 41: 1244–1256. https://doi.org/10.1016/j.cemconres.2010.12.001

[13] M. C. G. Juenger, R. Siddique, Recent advances in understanding the role of supplementary cementitious materials in concrete. Cem Concr Res (2015) 78: 71–80. https://doi.org/10.1016/j.cemconres.2015.03.018

[14] C. Meyer, The greening of the concrete industry. Cem Concr Compos (2009) 31: 601–605. https://doi.org/10.1016/j.cemconcomp.2008.12.010

[15] M. L. Berndt, Properties of sustainable concrete containing fly ash, slag and recycled concrete aggregate. Constr Build Mater (2009) 23: 2606–2613. https://doi.org/10.1016/j.conbuildmat.2009.02.011

[16] T. Oey, J. Timmons, P. Stutzman, J. W. Bullard, M. Balonis, M. Bauchy, G. Sant, An improved basis for characterizing the suitability of fly ash as a cement replacement agent. J Am Ceram Soc (2017) 100: 4785–4800. https://doi.org/10.1111/jace.14974

[17] T. Oey, A. Kumar, I. Pignatelli, Y. Yu, N. Neithalath, J.W. Bullard, M. Bauchy, G. Sant, Topological controls on the dissolution kinetics of glassy aluminosilicate. J Am Ceram Soc (2017) 100(12): 5521-5527.https://doi.org/10.1111/jace.15122

[18] S. Diamond, A review of alkali-silica reaction and expansion mechanisms 1. alkalies in cements and in concrete pore solutions. Cem Concr Res (1975) 5: 329–345. https://doi.org/10.1016/0008-8846(75)90089-7

[19] J. M. Ponce, O. R. Batic, Different manifestations of the alkali-silica reaction in concrete according to the reaction kinetics of the reactive aggregate. Cem Concr Res (2006) 36: 1148–1156. https://doi.org/10.1016/j.cemconres.2005.12.022

[20] L. S. Dent Glasser, N. Kataoka, The chemistry of "alkali-aggregate" reaction. Cem Concr Res (1981) 11: 1–9. https://doi.org/10.1016/0008-8846(81)90003-X

[21] F. P. Glasser, J. Marchand, E. Samson, Durability of concrete — degradation phenomena involving detrimental chemical reactions. Cem Concr Res (2008) 38: 226–246. https://doi.org/10.1016/j.cemconres.2007.09.015

[22] ASTM C618-15 Standard Specification for Coal Fly Ash and Raw or Calcined Natural Pozzolan for Use in Concrete, ASTM International, West Conshohocken, PA, (2015). https://doi.org/10.1520/C0618-15

[23] Http://www.mtixtl.com/, Last Accessed April 2015.

[24] B. Wang, Y. Yu, I. Pignatelli, G. Sant, M. Bauchy, Nature of radiation-induced defects in quartz. J Chem Phys (2015) 143: 24505. https://doi.org/10.1063/1.4926527

[25] https://www.wardsci.com/Store/.

[26] B. Wang, N. M. A. Krishnan, Y. Yu, M. Wang, Y. L. Pape, G. Sant, M. Bauchy, Irradiation-induced topological transition in sio2: structural

signature of networks' rigidity. J Non-Cryst Solids (2017) 463: 25–30. https://doi.org/10.1016/j.jnoncrysol.2017.02.017
[27] T. Oey, I. Pignatelli, M. Wang, E. Callagon, Y. H. Hsiao, M. Smedskajer, M. Bauchy, G. Sant, Atomic network topology reveals kinetic controls on the dissolution of boro-, alumino-, and alkali-silicate glasses and minerals. J. Chem. Phys. C (2017, submitted)
[28] T. Oey, K. Yang, J. W. Bullard, M. Bauchy, G. Sant, Topological controls on the dissolution kinetics of synthetic calcium aluminosilicate glasses. J. Am. Ceram. Soc. (2017, submitted)
[29] V. H. Rotberg, O. Toader, G. S. Was, I. L. Morgan, J. L. Duggan, M. Hall, A high intensity radiation effects facility. AIP Conf Proc (2001) 576: 687–691.
[30] R. E. Stoller, M. B. Toloczko, G. S. Was, A. G. Certain, S. Dwaraknath, F. A. Garner, On the use of srim for computing radiation damage exposure. Nucl Instrum Methods Phys Res, Sect B (2013) 310: 75–80.
[31] A. Kumar, J. Reed, G. Sant, Vertical scanning interferometry: a new method to measure the dissolution dynamics of cementitious minerals. J Am Ceram Soc (2013) 96: 2766–2778. https://doi.org/10.1111/jace.12482
[32] I. Pignatelli, A. Kumar, K. G. Field, B. Wang, Y. Yu, Y. Le Pape, M. Bauchy, G. Sant, Direct experimental evidence for differing reactivity alterations of minerals following irradiation: the case of calcite and quartz. Sci Rep (2016) 6: 20155. https://doi.org/10.1038/srep20155
[33] A. Luttge, U. Winkler, A. C. Lasaga, Interferometric study of the dolomite dissolution: a new conceptual model for mineral dissolution. Geochim Cosmochim Acta (2003) 67: 1099–1116. https://doi.org/10.1016/S0016-7037(02)00914-6
[34] R. S. Arvidson, I. E. Ertan, J. E. Amonette, A. Luttge, Variation in calcite dissolution rates: geochim. Cosmochim Acta (2003) 67: 1623–1634. https://doi.org/10.1016/S0016-7037(02)01177-8
[35] I. Pignatelli, A. Kumar, M. Bauchy, G. Sant, Topological control on silicates' dissolution kinetics. Langmuir (2016) 32: 4434–4439. https://doi.org/10.1021/acs.langmuir.6b00359
[36] I. Pignatelli, A. Kumar, R. Alizadeh, Y. Le Pape, M. Bauchy, G. Sant, A Dissolution-precipitation mechanism is at the origin of concrete creep in moist environments. J Chem Phys (2016) 145: 54701. https://doi.org/10.1063/1.4955429
[37] I. Pignatelli, A. Kumar, K. Shah, M. Balonis, M. Bauchy, B. Wu, G. Sant, Vertical Scanning Interferometry: A new method to quantify re-/de-mineralization dynamics of dental enamel. Dent Mater (2016) 32: 251–261. https://doi.org/10.1016/j.dental.2016.07.004
[38] Y-H. Hsiao, E. C. La Plante, N. M. A. Krishnan, Y. Le Pape, N. Neithalath, M. Bauchy, G. Sant, Effects of irradiation on albite's chemical durability. J Chem Phys C (2017, submitted)
[39] V. G. Papadakis, Effect of fly ash on Portland cement systems. Cem Concr Res (1999) 29: 1727–1736. https://doi.org/10.1016/S0008-8846(99)00153-2
[40] V. G. Papadakis, Effect of fly ash on Portland cement systems. Cem Concr Res (2000) 30: 1647–1654. https://doi.org/10.1016/S0008-8846(00)00388-4
[41] P. M. Dove, N. Han, A. F. Wallace, J. J. D. Yoreo, Kinetics of amorphous silica dissolution and the paradox of the silica polymorphs. Proc Natl Acad Sci (2008) 105: 9903–9908. https://doi.org/10.1073/pnas.0803798105
[42] S. L. Brantley, Kinetics of Mineral Dissolution. In Kinetics of Water-Rock Interaction. Springer New York, (2008): 151–210. https://doi.org/10.1007/978-0-387-73563-4_5
[43] A. C. Lasaga, A. Luttge, Variation of crystal dissolution rate based on a dissolution stepwave model. Science (2001) 291: 2400–2404. https://doi.org/10.1126/science.1058173
[44] D. Nečas, P. Klapetek, Gwyddion: An open-source software for spm data analysis. Open Phys (2011) 10: 181–188.
[45] L. Levien, C. T. Prewitt, D. J. Weidner, Structure and elastic properties of quartz at pressure. Am Mineral (1980) 65: 920–930.
[46] S. Plimpton, Fast Parallel Algorithms for Short-Range Molecular Dynamics. J Comput Phys (1995) 117 (1): 1-19. https://doi.org/10.1006/jcph.1995.1039
[47] M. Bauchy, Structural, Vibrational, and elastic properties of a calcium aluminosilicate glass from molecular dynamics simulations: the role of the potential. J Chem Phys (2014) 141: 24507. https://doi.org/10.1063/1.4886421
[48] C. Massobrio, J. Du, M. Bernasconi, P. S. Salmon, Molecular dynamics simulations of disordered materials. Springer (2015).
[49] N. M. A. Krishnan, B. Wang, Y. Le Pape, G. Sant, M. Bauchy, Irradiation- vs. vitrification-induced disordering: the case of $\alpha$-quartz and glassy silica. J Chem Phys (2017) 146: 204502. https://doi.org/10.1063/1.4982944
[50] T. Armbruster, H. B. Buergi, M. Kunz, E. Gnos, S. Broenniman, C. Lienert, Variation of Displacement Parameters in Structure Refinements of Low Albite. Am. Mineral. (1990) 75 (1–2): 135–140.
[51] H. J. C. Berendsen, J. P. M. Postma, W. F. van Gunsteren, A. DiNola, J. R. Haak, Molecular dynamics with coupling to an external bath. J Chem Phys (1984) 81: 3684–3690. https://doi.org/10.1063/1.448118
[52] J.F. Ziegler, J.P. Biersack, U. Littmark; The stopping and ranges of ions in solids, Pergamon: New York (1985).
[53] J. C. Phillips, Topology of covalent non-crystalline solids i: short-range order in chalcogenide alloys. J Non-Cryst Solids (1979) 34: 153–181. https://doi.org/10.1016/0022-3093(79)90033-4
[54] J. C. Mauro, Topological constraint theory of glass. Am Ceram Soc Bull (2011) 90: 31–37.
[55] M. Micoulaut, Y. Yue, Material functionalities from molecular rigidity: maxwell's modern legacy. MRS Bull (2017) 42 (1): 18–22. https://doi.org/10.1557/mrs.2016.298
[56] M. Bauchy, Topological constraints and rigidity of network glasses from molecular dynamics simulations. ArXiv150606483 Cond-Mat (2015).
[57] M. Bauchy, M. Micoulaut, Atomic scale foundation of temperature-dependent bonding constraints in network glasses and liquids. J Non-Cryst Solids (2011) 357: 2530–2537. https://doi.org/10.1016/j.jnoncrysol.2011.03.017
[58] M. M. Smedskjaer, J. C. Mauro, Y. Yue, Prediction of glass hardness using temperature-dependent constraint theory. Phys Rev Lett (2010) 105: 115503. https://doi.org/10.1103/PhysRevLett.105.115503
[59] M. Bauchy, M. J. A. Qomi, C. Bichara, F. J. Ulm, R. J. M. Pellenq, Rigidity transition in materials: hardness is driven by weak atomic constraints. Phys Rev Lett (2015) 114: 125502. https://doi.org/10.1103/PhysRevLett.114.125502
[60] G. J. Frischat, Ionic diffusion in oxide glasses. Trans Tech Publ. (1975).
[61] J. P. Hamilton, Corrosion behavior of sodium aluminosilicate glasses and crystals. PhD Thesis (1999).
[62] J. P. Hamilton, S. L. Brantley, C. G. Pantano, L. J. Criscenti, J. D. Kubicki, Dissolution of nepheline, jadeite and albite glasses: toward better models for aluminosilicate dissolution. Geochim Cosmochim Acta (2001) 65: 3683–3702. https://doi.org/10.1016/S0016-7037(01)00724-4
[63] K. L. Ngai, S. W. Martin, Correlation between the activation enthalpy and kohlrausch exponent for ionic conductivity in oxide glasses. Phys Rev B (1989) 40: 10550–10556. https://doi.org/10.1103/PhysRevB.40.10550
[64] A. J. Moulson, J. P. Roberts, Water in silica glass. Trans Faraday Soc (1961) 57: 1208. https://doi.org/10.1039/tf9615701208
[65] E. W. Shaffer, J. S. L. Sang, A. R. Cooper, A. H. Heuer, Diffusion of tritiated water in a-quartz. Sam by BJ Gjdleto H, A Yoder, RA 1, 131 (1974).
[66] T. Ichikawa, H. Koizumi, Possibility of radiation-induced degradation of concrete by alkali-silica reaction of aggregates. J Nucl Sci Technol (2002) 39: 880–884. https://doi.org/10.1080/18811248.2002.9715272
[67] T. Ichikawa, M. Miura, Modified model of alkali-silica reaction. Cem Concr Res (2007) 37: 1291–1297. https://doi.org/10.1016/j.cemconres.2007.06.008
[68] T. Ichikawa, T. Kimura, Effect of nuclear radiation on alkali-silica reaction of concrete. J Nucl Sci Technol (2007) 44: 1281–1284. https://doi.org/10.1080/18811248.2007.9711372
[69] Seabrook ASR-monitoring and building deformation aging management programs adult report, United States Nuclear Regulatory Commission (NRC) report, Washington, D.C. 20555-0001, Dec. 21, (2016).
[70] Concrete degradation by alkali-silica reaction, United States Nuclear Regulatory Commission (NRC) report, Washington, D.C. 20555-0001, Nov. 18, (2016).
[71] L. Douillard, J. P. Duraud, Swift Heavy Ion Amorphization of quartz — a comparative study of the particle amorphization mechanism of quartz. Nucl Instrum Methods Phys Res, Sect B (1996) 107: 212–217. https://doi.org/10.1016/0168-583X(95)01044-0
[72] L. L. Snead, S. J. Zinkle, J. C. Hay, M. C. Osborne, Amorphization of sic under ion and neutron irradiation. Nucl Instrum Methods Phys Res Sect B (1998) 141: 123–132. https://doi.org/10.1016/S0168-583X(98)00085-8